A quantitative model of glucose signaling in yeast reveals an incoherent feed forward loop leading to a specific, transient pulse of transcription

Sooraj Kuttykrishnan[a,b,1], Jeffrey Sabina[a,c,1], Laura L. Langton[a,b], Mark Johnston[a,c,2], and Michael R. Brent[a,b,c,3]

[a]Center for Genome Sciences and Systems Biology and Departments of [b]Computer Science and [c]Genetics, Washington University, St. Louis, MO 63130

Edited* by Jeffrey I. Gordon, Washington University School of Medicine, St. Louis, MO, and approved July 20, 2010 (received for review October 28, 2009)

The ability to design and engineer organisms demands the ability to predict kinetic responses of novel regulatory networks built from well-characterized biological components. Surprisingly, few validated kinetic models of complex regulatory networks have been derived by combining models of the network components. A major bottleneck in producing such models is the difficulty of measuring in vivo rate constants for components of complex networks. We demonstrate that a simple, genetic approach to measuring rate constants in vivo produces an accurate kinetic model of the complex network that *Saccharomyces cerevisiae* employs to regulate the expression of genes encoding glucose transporters. The model predicts a transient pulse of transcription of *HXT4* (but not *HXT2* or *HXT3*) in response to addition of a small amount of glucose to cells, an outcome we observed experimentally. Our model also provides a mechanistic explanation for this result: *HXT2–4* are governed by a type 2, incoherent feed forward regulatory loop involving the Rgt1 and Mig2 transcriptional repressors. The efficiency with which Rgt1 and Mig2 repress expression of each *HXT* gene determines which of them have a pulse of transcription in response to glucose. Finally, the model correctly predicts how lesions in the feed forward loop change the kinetics of induction of *HXT4* expression.

gene–regulatory networks | glucose transport | kinetic model | *Saccharomyces cerevisiae* | systems biology

Quantitative models of gene regulatory networks typically serve one of two distinct purposes. One is to determine whether a qualitative model adequately describes the biological network (1, 2). When qualitative model checking is the goal, no claims are made about the accuracy of the kinetic or thermodynamic parameters that describe molecular interactions; plausible values, which may be based on general principles or on published measurements of plausibly related quantities, are typically used. The second, less frequently pursued goal is to produce a model that predicts the behavior of a complex system on the basis of accurate quantitative models of its components. Such models can be used to predict the quantitative behavior of novel, engineered systems built by rewiring the components of the original system into new circuits. An excellent example of this component-based approach is the model of the network determining the lysis/lysogeny decision of phage λ (3–5). In that case, simulations of the stochastic interactions of individual molecules were carried out, allowing the frequency of each outcome (lysis or lysogeny) in isogenic populations to be explained quantitatively (4). The level of detail in that model was possible because of the enormous effort devoted to biochemical studies of each component of phage λ. As a result, this approach cannot easily be applied to other complex networks.

We describe a simple approach to kinetic modeling and demonstrate that it yields accurate predictions of the behavior of a complex regulatory network. We modeled the Snf/Rgt/Mig (SRM) glucose-sensing network of *Saccharomyces cerevisiae* (Fig. 1), which governs expression of *HXT* genes encoding glucose transporters. A clear qualitative model of this network has emerged (6–8), based on steady-state data. However, a molecular understanding of the kinetic responses of such systems is necessary for the engineering of biological pathways to perform new functions. The kinetic responses of biological systems can also be critical for fitness. Cells that do not react quickly enough to changing nutrient conditions risk being overgrown by competitors that are quicker on the uptake. Those that respond too quickly risk wasting energy on the response itself and being overgrown by more efficient competitors (9). Because response kinetics have profound consequences for the cell, we sought to move beyond a steady-state description by developing a detailed kinetic model of the SRM network. We used the model to make predictions and guide the design of experiments that provide unique mechanistic insights into this system.

The Snf/Rgt/Mig (SRM) Network. The SRM network consists of two signal transduction pathways. The first is the glucose sensing pathway that leads to induction of *HXT* genes in response to glucose (Fig. 1, green lines). An intracellular signal is generated when glucose binds to the Snf3 and Rgt2 sensors at the membrane, which leads to degradation of Mth1 and Std1. Disappearance of Mth1 and Std1 results in inactivation of the Rgt1 transcriptional repressor and derepression of its targets, including *HXT* genes and the genes encoding Mth1, Std1, and Mig2.

The second pathway in the SRM network causes repression of gene expression in response to glucose (Fig. 1, red lines) mediated by the Mig1 transcriptional repressor. Glucose metabolism leads to inhibition of the Snf1 protein kinase (10), thus preventing it from phosphorylating Mig1. Hypophosphorylated Mig1 moves into the nucleus and represses its many targets (11), including *HXT2*, *HXT3*, and *HXT4*.

These glucose induction and repression pathways are highly interconnected (Fig. 1), with eight regulatory genes at the core of the network. All but three of them (*SNF1, RGT1*, and *RGT2*) are regulated by one or both pathways (Fig. 1, color-coded ovals), forming several feed forward and feedback loops. For example, both Rgt1 and Mig1/Mig2 regulate expression of *MTH1*, which acts in the glucose induction pathway. This degree of connectedness of the SRM network—more complex than the well-characterized *GAL* gene regulatory network, but well below the level of complexity of the cell cycle regulatory network—makes modeling it a challenging but tractable goal.

The model we describe is based on kinetic parameters for the components of the SRM network, most of which have been directly measured as described below. We use transcription rate equations whose parameters we measured at steady state. Most of the other

Author contributions: S.K., J.S., M.J., and M.R.B. designed research; S.K., J.S., and L.L.L. performed research; S.K. analyzed data; and S.K., J.S., M.J., and M.R.B. wrote the paper.

The authors declare no conflict of interest.

*This Direct Submission article had a prearranged editor.

[1]S.K. and J.S. contributed equally to this work.

[2]Present address: Department of Biochemistry and Molecular Genetics, University of Colorado at Denver, Aurora, CO 80045.

[3]To whom correspondence should be addressed. E-mail: brent@wustl.edu.

This article contains supporting information online at www.pnas.org/lookup/suppl/doi:10.1073/pnas.0912483107/-/DCSupplemental.

SYSTEMS BIOLOGY

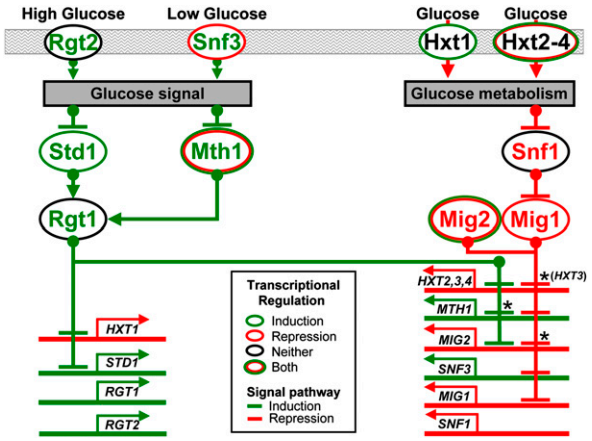

Fig. 1. Qualitative model of the SRM, showing the glucose induction pathway (green lines) and the glucose repression pathway (red lines). Colored ovals indicate which pathways regulate transcription of the mRNA for each protein (green, induction; red, repression; black, neither one). Each gene is color coded for the pathway in which its product serves. Three of the repression relationships marked with an asterisk (Mig1 on *HXT3* and *MIG2* and Rgt1 on *MTH1*) were revealed as a result of the experiments described here.

parameters (mRNA half-lives, translation rates, and protein half-lives) have been directly measured before (12–16).

Results

Kinetic Model. We wrote a set of ordinary differential equations (ODEs) that describe the rate of change in the concentration of each molecular species appearing in Fig. 1 (see Tables S1 and S2 for the full set of ODEs and Tables S3 and S4 for parameter values). The ODEs are based on rate equations for each of six types of reactions: transcription, translation, degradation of mRNAs, degradation of proteins, protein–protein binding, and phosphorylation of proteins. Translation and degradation are modeled as irreversible mass action reactions. Protein–protein binding and phosphorylation reactions are modeled as fast reactions (quasi-equilibrium assumption, ref. 17).

Following Goutsias and Kim (18), we modeled the rate of change of the concentration of an mRNA regulated by repressors $R_{1,\ldots,n}$ using the equation

$$\frac{d\,[\mathrm{mRNA}]}{dt} = V_{\max} \prod_{i=1}^{n} \frac{1}{1+\theta_i[R_i]} - k[\mathrm{mRNA}], \qquad [1]$$

where brackets denote concentrations, $V_{\max}$ is the transcription rate in the absence of all repressors, θ_i is the efficiency with which repressor R_i represses transcription of a particular gene (one over the concentration required for half-maximal repression), and k is the degradation rate of a particular mRNA. As the concentration of any repressor decreases, the rate of transcription given by the equation will monotonically increase and saturate; as the level of any repressor increases, the transcription rate monotonically decreases, approaching zero. The model of transcriptional activation, which occurs only between Rgt1 and *HXT1*, is described in *Methods*.

Two approximations about *cis*-regulation are made in this model: (*i*) The net effect of all binding sites of the repressor in each promoter is modeled as a single pseudobinding site and (*ii*) each repressor influences transcription independently (18, 19). In other words, the model does not include cooperative binding within or between repressors. We adopted these simplifying approximations on the grounds that greater complexity and more parameters can easily be added to the model when there are sufficient data to determine those parameters (*Discussion*).

Preliminary Tests of Steady-State Predictions Reveal Unforeseen Regulatory Interactions. Preliminary tests of the model revealed three significant discrepancies between predicted and observed patterns of *HXT* gene expression. We were able to correct these by adding the three regulatory relationships marked by asterisks in Fig. 1 (see Fig. S1 for detailed logic), one of which was independently discovered during the course of this work (20).

Estimating the Parameters of Model Components. The measurements made in this study, along with those made in previous high-throughput studies, were used to calculate higher-order parameters (*e.g.*, $V_{\max}$, θ) necessary for modeling transcription and translation (Fig. 2*A* and *Methods*). In this manner we were able to calculate 81 parameters from direct experimental measurements (Fig. 2*B*). Because the parameters of the two sensors, Rgt2 and Snf3, could not be measured directly, we used a one-sensor model, reducing the number of genes in the system from 12 to 11. Simulations suggested that this had no significant effect on predictions. The 10 remaining parameters were chosen by optimizing the fit between the model predictions and experimentally measured steady-state levels of *HXT1–4* mRNA in wild-type and mutant cells (see Table S5 for information about the strains) grown on 2% galactose or on

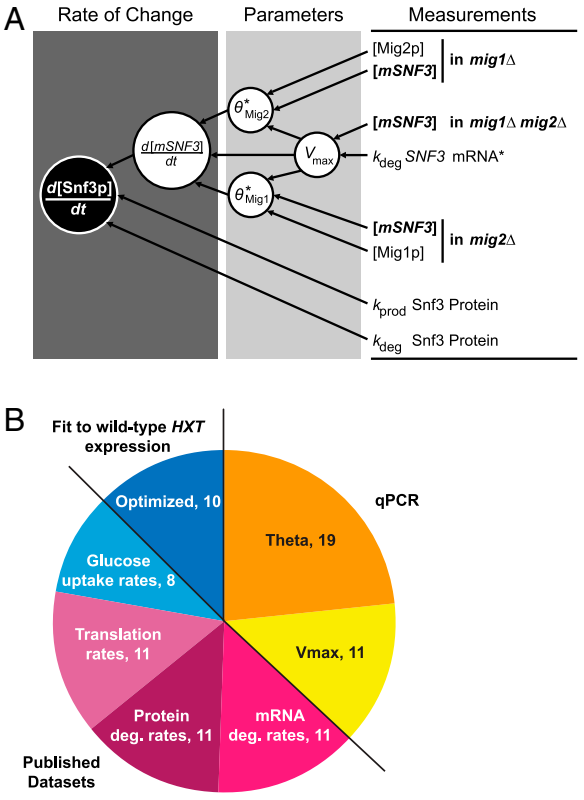

Fig. 2. (*A*) Contributions made by each measurement to the parameters describing the rates of change of *mSNF3* (white circles) and Snf3p (black circle). Measurements made during the course of this study (boldface type) and those taken from literature sources are depicted on the *Right*. Information flow, beginning with measured quantities, is shown by the arrows as it is used to calculate higher-order parameters. The degradation rate constant k_{deg}, in addition to its contribution to $V_{\max}$, is also used directly in the calculation of each value for θ, indicated by an asterisk. Protein abundances in mutants were estimated by simulation, using translation rates calculated from steady-state protein abundances in wild-type yeast. (*B*) Translation rates, protein degradation rates, and mRNA degradation rates were obtained from publicly available high-throughput data (12, 15, 16). Glucose uptake rates were obtained from ref. 32. $V_{\max}$ and θ were calculated from mRNA expression measurements using qPCR and protein abundance data (13, 14).

2% glucose (56 data points). To avoid overfitting the 10 optimized parameters, the prediction for each data point was made by holding that point out and using a model in which the optimized parameters were fit to the other 55 data points. The resulting model was used to predict the held-out point. The range of parameter values from each of the 56 optimizations was relatively tight (Table S6), suggesting that the parameters are reasonably well determined.

Testing Steady-State Predictions. To test the model, steady-state mRNA levels of *HXT1–4* were simulated for cells growing in 2% galactose or in 2% glucose and measured experimentally (Fig. 3). The predictions are in good agreement with steady-state mRNA levels determined by qPCR, provided their relative abundance is at least 1 (a value that we estimate to be ~1 molecule/cell assuming that the abundance of actin mRNA is ~81 molecules/cell) (21). When the observed level is <1, the largest predicted value is 2.28 (m*HXT4* in *std1Δ* in 2% glucose). When the observed level is at least 1, the two largest differences between observation and prediction were 1.19-fold (m*HXT4* in *std1Δ* in 2% glucose) and 0.86-fold (m*HXT3* in *mth1Δ* in 2% galactose); the remaining observations were all within 10% of the predicted values. Because each data point was predicted using parameters optimized without considering that point, these results cannot be explained by overfitting of parameters. (Note that the red points in Fig. 3 were used in algebraic computation of V_{max} and θ parameters, which were not optimized.)

Sensitivity of Model Predictions to Parameter Values. To get a sense of which parameters the predictions are most sensitive to, we varied each measured parameter by ±10% and plotted the predicted value for each of the four *HXT* mRNAs in each of the two conditions (2% glucose and 2% galactose). All of the plots were approximately linear. We then used their slopes as a measure of sensitivity. To rank the measured parameters in overall effect, we averaged the slopes over the four mRNAs and two conditions (Dataset S1 contains the complete results). Among the 19 repression efficiency parameters (θ's), by far the most important were those governing the effects of Rgt1 and Mig2 on transcription of *MTH1*. Among the 11 mRNA and 11 protein degradation rates, the most important were those associated with *MTH1*. Among maximal transcription rates, each *HXT* gene was significantly affected only by its own rate, and even then the effects were much smaller than those involving *MTH1*. Together, these observations point to *MTH1* as the keystone of the system (22). In general, *MIG2* is also more significant than *MIG1*. Although we did not anticipate these findings, they are consistent with the fact that *MTH1* and *MIG2* are the two genes that are regulated by both the glucose induction and repression pathways (Fig. 1) and repress one another (via their products).

Testing Kinetic Predictions After Glucose Addition. The predictive power of the model was assessed by simulating the kinetics of *HXT1–4* expression after addition of glucose to cells growing on galactose and then testing these predictions by direct measurements of mRNA. For *HXT1*, *HXT2*, *HXT3*, and *HXT4* the predictions for addition of 2% glucose were in good agreement with our experimental time courses (Fig. 4, red).

As a prospective test of the robustness of the model, we simulated the kinetics of *HXT* expression after addition of 0.1% glucose. Yeast cells are known to express a different complement of *HXT* genes under this "low glucose" condition than in 2% glucose (23). The minimal changes measured in expression of *HXT1–3* are in good agreement with the predictions of the model (Fig. 4 *A–C*, blue).

Prediction, Verification, and Explanation of the *HXT4* Pulse. The most interesting prediction of the model was that *HXT4* (and only *HXT4*) would display a transient pulse of expression after addition of 0.1% glucose (Fig. 4*D*, solid blue lines; Fig. S2 shows the robustness of this prediction to variation of key parameters). This prediction results from a feed forward loop in which *HXT4* is repressed by both Rgt1 and Mig2, and *MIG2* is itself repressed by Rgt1 (Fig. 5*A*; predicted kinetics of the active repressor proteins are shown in Fig. 5*B*). This network motif, called an incoherent feed forward loop (24), is known to be capable of generating a pulse, but only with certain parameters. In this case, *HXT4*, *HXT3*, and *HXT2* are all regulated by the same feed forward loop, but only *HXT4* is predicted to display a pulse. This was unexpected: Previous studies that assayed *HXT4* expression with a β-galactosidase reporter, a long-lived protein, failed to capture these dynamic changes in mRNA concentration (23). The existence of a pulse and the timing of its peak were confirmed by measuring the level of *HXT4* mRNA over the course of 2 h, although the height of the measured peak and the final level of *HXT4* mRNA differ from the prediction (Fig. 4*D*, blue).

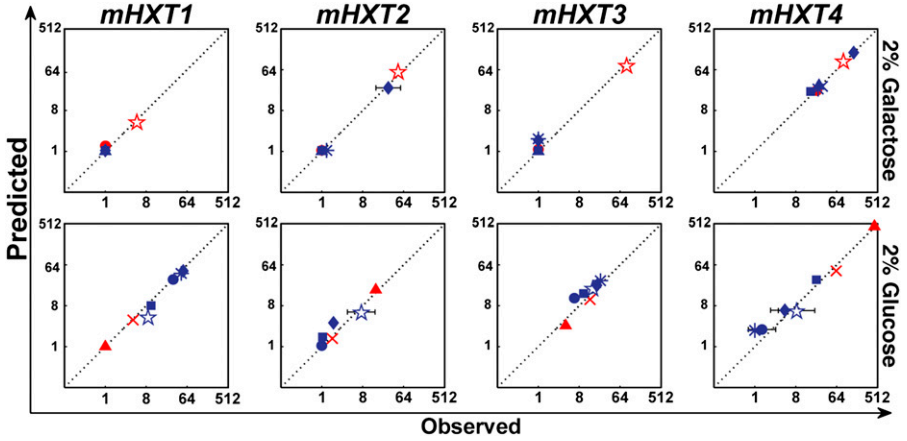

Fig. 3. Observed and predicted steady-state levels of *HXT1*, *HXT2*, *HXT3*, and *HXT4* mRNAs, relative to the level of *ACT1* in the same sample, when the cells were grown in 2% galactose (*Upper*) or 2% glucose (*Lower*). Units are molecules per 81 *ACT1* molecules, a rough estimate of the number of *ACT1* molecules in each yeast cell (21) (Dataset S2 contains all observed steady-state levels). Each data point represents a strain. Wild type is represented by circles, *rgt1Δ* by stars, *mth1Δ* by diamonds, *std1Δ* by asterisks, *mig1Δ* by crosses, *mig2Δ* by squares, and *mig1Δ mig2Δ* by triangles. Error bars indicating one SEM are present for the five empirical measurements with the largest errors; the smaller bars would not be clearly visible on this scale. The data points that were used to calculate V_{max} and θ are in red and the independent tests of the model are in blue. Each data point is predicted using a model whose optimized parameters are fit to the remaining data points. All observed values less than the threshold of our ability to reliably quantify using qPCR, 1 unit, were set to 1 unit.

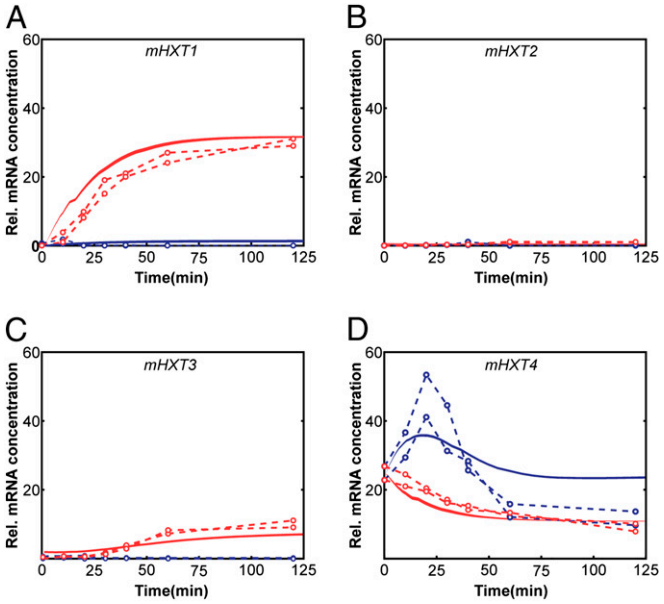

Fig. 4. Measured and predicted time courses for *mHXT1*, *mHXT2*, *mHXT3*, and *mHXT4* expression after glucose addition. Circles depict the levels of each mRNA observed (see Dataset S3 for all timecourse data) using qPCR after a shift from 2% galactose to 2% glucose (red line) or to 0.1% glucose (blue line). The lines are narrow solid regions that encompass the family of predictions derived from parameters estimated by randomly selecting among replicate measurements (*SI Methods*). This region represents the variation in the prediction caused by variation in the measurements used to estimate the parameters.

To further investigate the role of the feed forward loop in creating a pulse of *HXT4* expression, we ran kinetic simulations of *HXT4* mRNA levels for deletion mutants lacking one of the two regulatory components of the loop, Mig2 or Rgt1. Without Mig2 to repress *HXT4* after its initial derepression by Rgt1, the response to addition of 0.1% glucose was predicted to be a substantial increase in *HXT4* mRNA at steady state, and this was confirmed by quantitative (q)PCR (Fig. 5*C*). In the absence of Rgt1, the feed forward loop is no longer operative and *HXT4* is predicted to be highly expressed in galactose, where Mig2 (no longer repressed by Rgt1) is its only repressor. When 0.1% glucose is added, however, the rapid increase in active Mig1 is predicted to reduce transcription of *HXT4* mRNA, which decays over the next ~30 min. This predicted decrease, along with its level and timing, was confirmed by qPCR (Fig. 5*D*).

Discussion

To systematically design gene regulatory networks that meet predetermined specifications, we must have a catalog of well-characterized parts and be able to predict what will happen when those parts are wired together in specific ways. We have demonstrated the ability to characterize naturally occurring components and to combine those characterizations into a model that predicts the kinetic behavior of the Snf/Rgt/Mig network with satisfying accuracy. This network is complex, relative to other kinetically characterized networks: It integrates input from two signaling pathways via eight regulatory proteins that are linked by 11 transcriptional regulation relationships, which, together with direct protein–protein interactions, form multiple feedback and feed forward loops. This network regulates transcription of the four *HXT* genes via an additional 10 regulatory interactions.

We chose an intermediate point along the continuum from simple, abstract models with few parameters that are fully determined by available data to detailed physical models with many, realistic parameters that are highly underdetermined. A degree of simplification, abstraction, and global optimization was required at the tops of the two pathways (where we were not able to directly measure the binding of glucose to the receptors or quantify the signal from glucose metabolism). All of the points in Fig. 3 (which include the steady-state red points in Fig. 4) were used to globally optimize 10 parameters describing events occurring at the tops of the two pathways. To guard against overfitting, we evaluated model predictions using a hold-out strategy (Fig. 3). We also reduced the action of each repressor at each promoter to a single parameter, θ, representing its repression efficiency. We did not attempt to measure or model cooperative binding of repressors. Importantly, θ has a clear biochemical interpretation that is localized to a single repressor and a single target gene. This localization to specific components of the system is essential for the rational design of new networks using the same components. It also allowed us to measure V_{max} and θ by genetic isolation and perturbation, thus avoiding

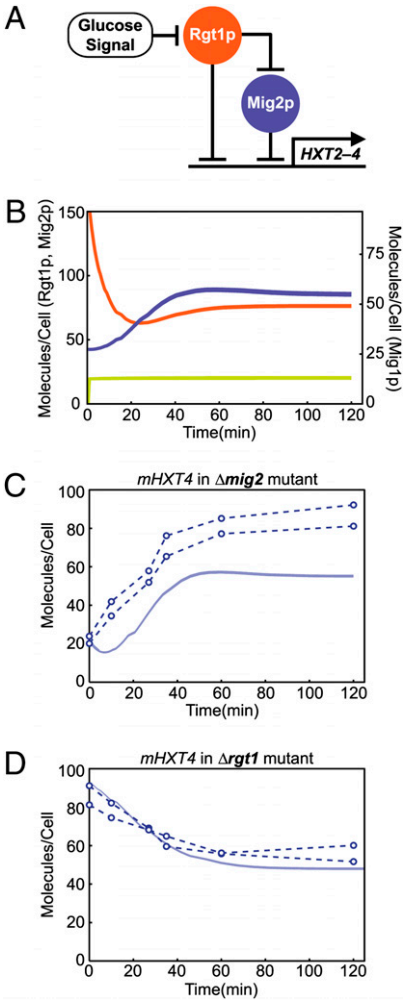

Fig. 5. (*A*) A schematic diagram of the type 2 incoherent feed forward loop regulating expression of *HXT2–4* (note that the driving signal from glucose is inhibitory). (*B*) Predicted levels of the three repressor proteins: Mig2 (blue), Rgt1 (orange), and Mig1 (green, right-hand scale). The model predicts a pulse of *HXT4* expression in part because Rgt1 drops off before Mig2 has risen to its steady-state level. (*C*) Circles, experimental time course of *HXT4* mRNA in *mig2Δ* cells after addition of 0.1% glucose to a galactose culture, measured by qPCR. Solid region, range of predicted *HXT4* mRNA in *mig2Δ* cells as in Fig. 4. (*D*) Circles, experimental time course of *HXT4* mRNA in *rgt1Δ* cells after addition of 0.1% glucose to a galactose culture, measured by qPCR. Solid region, range of predicted *HXT4* mRNA in *rgt1Δ* cells, obtained as in Fig. 4.

global optimization of transcriptional parameters. This measurement was facilitated by existing data on mRNA and protein half-lives and protein abundances in rich medium (which we combined to compute approximate translation rates). Seventy-one parameters (87%) were fully determined by previous datasets combined with our measurements in 2% galactose or 2% glucose.

Only after all model parameters and predictions were fixed did we carry out our experiments in 0.1% glucose (blue circles in Figs. 4 and 5). These data, along with the intermediate time points after addition of 2% glucose (red points, Fig. 4), constitute new challenges not used to calculate any parameters. Thus, discrepancies between prediction and observation in these cases represent either (*a*) measurement error (in our data or other datasets we used) or (*b*) structural error in the assumptions underlying the model. We chose to leave those discrepancies exactly as we found them, rather than reducing them by incorporating the new data into parameter estimation, to point the way to future research aimed at systematically addressing the measurement and/or structural error that underlies the discrepancies.

Our approach to obtaining direct measurements of transcriptional parameters is potentially applicable to a variety of other systems of similar complexity. In systems where gene deletion is difficult or impossible, expression of transcription factors can be modulated by methods such as RNA interference, although this method introduces a number of complexities that are not present when transcription factors can be cleanly removed. Furthermore, systems in which cooperative binding of transcription factors plays an important role require more complex experimental treatment. Finally, kinetic models depend on the half lives of mRNAs and proteins. In systems where these are already known, as they are for most yeast genes, kinetic modeling becomes significantly easier.

In the course of building the model, we learned that *HXT2*, *HXT3*, and *HXT4* are all regulated both by Mig1 and by a feed forward loop involving Rgt1 and Mig2. Previously, *HXT3* was not known to be repressed by Mig1 and Mig2. Using measured degradation rate constants together with transcriptional parameters determined solely from steady-state data, the model predicted correctly that *HXT4*, but not *HXT2* or *HXT3*, would display a transient pulse of expression after addition of 0.1% glucose to galactose-grown cells. It also predicted correctly than none of the other *HXT*s would display such a pulse after addition of 2% glucose. Finally, our model predicted with reasonable accuracy the kinetics of *HXT4* expression after addition of 0.1% glucose in mutants lacking *MIG1* or *RGT1*. These predictions could not have been made on the basis of the qualitative model alone, which does not reveal the differences in regulation of *HXT2*, *HXT3*, and *HXT4*. Differentiating *HXT4* from *HXT2* and *HXT3* absolutely required quantitative parameterization.

The pulse in *HXT4* expression, which peaks at two to three times the steady-state levels, is striking, but it is not yet clear what physiological benefits, if any, it confers. In general, a pulsed response may enable a cell to optimize the trade-off between rapid response to changing conditions and long-term energy efficiency. When the synthesis rate of an mRNA or a protein increases, the time required to reach steady state depends on its degradation rate constant, not on its rate of synthesis (24). A rapid shift in steady-state concentration requires an unstable molecule that must be constantly resynthesized, imposing a high energetic cost. However, a rapid, transient response, which imposes that energetic cost for only a short time, can buy time for a slower, steady-state response by a more stable molecule.

Ultimately, our goal is to be able to rationally design regulatory systems with specific kinetic characteristics. For example, to understand the physiological effects of the *HXT4* pulse, we might want to design a system that achieves the same steady-state expression levels at approximately the same rate, but without the pulse. The model presented here allows us to calculate the repression efficiency parameters for Rgt1, Mig1, and Mig2 on *HXT4* that would be required to produce such a response. To design the mutations needed to accomplish our desired response, however, one piece is missing: the ability to predict the repression efficiency parameters from the affinities and locations of all of a repressor's binding sites in a given promoter. In other words, we need a more detailed physical model of the action of each repressor at each promoter. Recent progress in linking the ensemble of binding sites to the overall effect of the transcription factor (20, 25), combined with quantitative, kinetic models such as the one presented here, puts us on the road to de novo design of systems producing complex kinetic phenotypes.

Methods

Parameters That Were Specifically Measured in Previous High-Throughput Studies. Multiple genome-wide studies of mRNA decay in *S. cerevisiae* provide degradation rates of all of the mRNAs in the network (15, 16). In this initial model, we approximated mRNA degradation rates as constants that do not depend on the glucose concentration. It is known that several mRNAs encoding proteins involved in the TCA cycle and in gluconeogenesis exhibit glucose-dependent changes in decay (26–28) but there is as yet no evidence that this affects mRNAs in our network. Degradation rate constants for the protein species in the network were taken from the results of Belle and colleagues (12). In that study, Hxt1–4 were determined to have half-lives >300 min, so we used that lower bound as an approximation to their half-lives.

Estimating Parameters from Data. The V_{max} for each promoter and the value of θ for each repressor acting at that promoter were calculated using mRNA concentrations determined by quantitative PCR (qPCR; *SI Methods*). To isolate the effects of each parameter, measurements were made in carefully selected mutants and growth conditions (Fig. 2*A Right*). For example, transcription of *SNF3* mRNA (*mSNF3*) is repressed by both Mig1 and Mig2, so Eq. **1** becomes

$$\frac{d\,[mSNF3]}{dt} = V_{\max}\left(\frac{1}{1+\theta_{Mig1-SNF3}[\mathrm{Mig1}]}\right) \times \left(\frac{1}{1+\theta_{Mig2-SNF3}[\mathrm{Mig2}]}\right) - k_{\deg}\,[mSNF3]. \quad \textbf{[2]}$$

At steady state, the rate of change of *SNF3* mRNA is zero, and in a *mig1*Δ *mig2*Δ double mutant, the concentrations of Mig1 and Mig2 are also zero. Thus, $V_{max} = k_{deg}[mSNF3]$. The degradation rate of *SNF3* mRNA, k_{deg}, is available from the studies cited above; we measured the concentration of *SNF3* mRNA, in a *mig1*Δ *mig2*Δ mutant.

With V_{max} in hand, we calculated the θ for each repressor in a single mutant. To calculate $\theta_{Mig1-SNF3}$, for example, we used a *mig2*Δ mutant, where, at steady state

$$0 = V_{\max}\left(\frac{1}{1+\theta_{Mig1-SNF3}[\mathrm{Mig1}]}\right) - k_{\deg}\,[mSNF3]. \quad \textbf{[3]}$$

Solving for $\theta_{Mig1-SNF3}$ yields

$$\theta_{Mig1-SNF3} = \left(\frac{V_{\max}}{k_{\deg}[mSNF3]} - 1\right)\cdot\left(\frac{1}{[\mathrm{Mig1}]}\right). \quad \textbf{[4]}$$

So the efficiency with which Mig1 represses *SNF3* expression is estimated from V_{max} and the steady-state concentrations of *mSNF3* and Mig1 (Fig. 2). The steady-state concentration of *mSNF3* in the *mig2Δ* strain was measured by qPCR.

To obtain [Mig1] we took advantage of multiple genome-wide studies (13, 29, 30) that provide estimates of abundance for most proteins in *S. cerevisiae* growing in yeast extract/peptone and glucose (Fig. 2*A* and its legend). Similarly, by combining steady-state levels of *mSNF3* in a *mig1*Δ strain with estimates of [Mig2] abundance from genome-wide studies, we calculated $\theta_{Mig2-SNF3}$.

Regulation of *HXT1* Transcription. Rgt1 is known to act as a transcriptional activator of *HXT1* when glucose is present (31). So we model the transcription of *HXT1* by the equation

$$\frac{d[mHXT1]}{dt} = V_{HXT1}\cdot\left(T_{HXT1} + \frac{(1-T_{HXT1})\theta_{\text{activation}}[\text{Glucose signal}][Rgt1]}{1+\theta_{\text{activation}}[\text{Glucose signal}][Rgt1]}\right) \cdot\left(\frac{1}{1+\theta_{\text{Active}\,Rgt1-HXT1}\left([Rgt1:Mth1]+[Rgt1:Std1]\right)}\right) - k[HXT1], \quad [5]$$

where V_{HXT1} is the transcription rate of *HXT1* when both Mth1 and Std1 are absent and Rgt1 is present in excess, T_{HXT1} is a scaling factor for the basal transcription rate of *HXT1* (unitless), $\theta_{\text{activation}}$ is the efficiency with which Rgt1 activates the expression of the *HXT1* gene in the presence of a glucose-induced signal, $\theta_{\text{Active }Rgt1-HXT1}$ is the efficiency with which active Rgt1 which is either a Rgt1:Mth1 dimer or a Rgt1:Std1 dimer represses the expression of the *HXT1* gene, and k is the degradation rate of *mHXT1*.

Parameter Optimization. Each of the 10 parameters that could not be measured directly was fit to steady-state levels of *mHXT1*, *-2*, *-3*, and *4* in seven different strains (wild type, *rgt1Δ*, *mth1Δ*, *std1Δ*, *mig1Δ*, *mig2Δ*, and *mig1Δ mig2Δ*), when cells were grown in 2% galactose or in 2% glucose (56 data points in total). Optimization was carried out in MatLab using the function "lsqnonlin" with trust-region-reflective algorithm.

ACKNOWLEDGMENTS. We thank A. Kaniak (Institute of Biochemistry and Biophysics, Polish Academy of Sciences, Warsaw, Poland) for unpublished strains and Barak Cohen for useful conversations. This work was supported by National Institutes of Health Grant GM32540 (to M.J.) and by funding from Washington University. J.S. was supported by National Research Service Award postdoctoral fellowship GM076967. S.K. was supported by National Human Genome Research Institute Grant T32 HG000045.

1. Chen KC, et al. (2004) Integrative analysis of cell cycle control in budding yeast. *Mol Biol Cell* 15:3841–3862.
2. Tyson JJ, Novak B (2008) Temporal organization of the cell cycle. *Curr Biol* 18: R759–R768.
3. Shea MA, Ackers GK (1985) The OR control system of bacteriophage lambda. A physical-chemical model for gene regulation. *J Mol Biol* 181:211–230.
4. Arkin A, Ross J, McAdams HH (1998) Stochastic kinetic analysis of developmental pathway bifurcation in phage lambda-infected Escherichia coli cells. *Genetics* 149: 1633–1648.
5. McAdams HH, Arkin A (1997) Stochastic mechanisms in gene expression. *Proc Natl Acad Sci USA* 94:814–819.
6. Coons DM, Vagnoli P, Bisson LF (1997) The C-terminal domain of Snf3p is sufficient to complement the growth defect of snf3 null mutations in Saccharomyces cerevisiae: SNF3 functions in glucose recognition. *Yeast* 13:9–20.
7. Kaniak A, Xue Z, Macool D, Kim JH, Johnston M (2004) Regulatory network connecting two glucose signal transduction pathways in Saccharomyces cerevisiae. *Eukaryot Cell* 3:221–231.
8. Flick KM, et al. (2003) Grr1-dependent inactivation of Mth1 mediates glucose-induced dissociation of Rgt1 from HXT gene promoters. *Mol Biol Cell* 14:3230–3241.
9. Kalisky T, Dekel E, Alon U (2007) Cost-benefit theory and optimal design of gene regulation functions. *Phys Biol* 4:229–245.
10. Wilson WA, Hawley SA, Hardie DG (1996) Glucose repression/derepression in budding yeast: SNF1 protein kinase is activated by phosphorylation under derepressing conditions, and this correlates with a high AMP:ATP ratio. *Curr Biol* 6:1426–1434.
11. De Vit MJ, Waddle JA, Johnston M (1997) Regulated nuclear translocation of the Mig1 glucose repressor. *Mol Biol Cell* 8:1603–1618.
12. Bekke AM, Tanay A, Bitincka L, Shamir R, O'Shea EK (2006) Quantification of protein half-lives in the budding yeast proteome. *Proc Natl Acad Sci USA* 103:13004–13009.
13. Ghaemmaghami S, et al. (2003) Global analysis of protein expression in yeast. *Nature* 425:737–741.
14. Lu P, Vogel C, Wang R, Yao X, Marcotte EM (2007) Absolute protein expression profiling estimates the relative contributions of transcriptional and translational regulation. *Nat Biotechnol* 25:117–124.
15. Wang Y, et al (2002) Precision and functional specificity in mRNA decay. *Proc Natl Acad Sci USA* 99 (9):5860–5865.
16. Holstege FC, et al. (1998) Dissecting the regulatory circuitry of a eukaryotic genome. *Cell* 95:717–728.
17. Saucerman JJ, McCulloch AD (2004) Mechanistic systems models of cell signaling networks: A case study of myocyte adrenergic regulation. *Prog Biophys Mol Biol* 85: 261–278.
18. Goutsias J, Lee NH (2007) Computational and experimental approaches for modeling gene regulatory networks. *Curr Pharm Des* 13:1415–1436.
19. Goutsias J, Kim S (2004) A nonlinear discrete dynamical model for transcriptional regulation: Construction and properties. *Biophys J* 86:1922–1945.
20. Gertz J, Siggia ED, Cohen BA (2009) Analysis of combinatorial cis-regulation in synthetic and genomic promoters. *Nature* 457:215–218.
21. Velculescu VE, et al. (1997) Characterization of the yeast transcriptome. *Cell* 88: 243–251.
22. Sabina J, Johnston M (2009) Asymmetric signal transduction through paralogs that comprise a genetic switch for sugar sensing in Saccharomyces cerevisiae. *J Biol Chem* 284:29635–29643.
23. Ozcan S, Johnston M (1995) Three different regulatory mechanisms enable yeast hexose transporter (HXT) genes to be induced by different levels of glucose. *Mol Cell Biol* 15:1564–1572.
24. Kaplan S, Bren A, Dekel E, Alon U (2008) The incoherent feed-forward loop can generate non-monotonic input functions for genes. *Mol Syst Biol* 4:203.
25. Segal E, Raveh-Sadka T, Schroeder M, Unnerstall U, Gaul U (2008) Predicting expression patterns from regulatory sequence in Drosophila segmentation. *Nature* 451:535–540.
26. Bennett MR, et al. (2008) Metabolic gene regulation in a dynamically changing environment. *Nature* 454:1119–1122.
27. Kresnowati MT, et al. (2006) When transcriptome meets metabolome: Fast cellular responses of yeast to sudden relief of glucose limitation. *Mol Syst Biol* 2:49.
28. Yin Z, Hatton L, Brown AJ (2000) Differential post-transcriptional regulation of yeast mRNAs in response to high and low glucose concentrations. *Mol Microbiol* 35: 553–565.
29. Lu P, Vogel C, Wang R, Yao X, Marcotte EM (2007) Absolute protein expression profiling estimates the relative contributions of transcriptional and translational regulation. *Nat Biotechnol* 25:117–124.
30. Newman JR, Jr, et al. (2006) Single-cell proteomic analysis of S. cerevisiae reveals the architecture of biological noise. *Nature* 441:840–846.
31. Polish JA, Kim JH, Johnston M (2005) How the Rgt1 transcription factor of Saccharomyces cerevisiae is regulated by glucose. *Genetics* 169:583–594.
32. Reifenberger E, Boles E, Ciriacy M (1997) Kinetic characterization of individual hexose transporters of Saccharomyces cerevisiae and their relation to the triggering mechanisms of glucose repression. *Eur J Biochem* 245:324–333.